92-009

Wat. Sci. Tech. Vol. 26, No. 3-4, pp. 577–584, 1992.
Printed in Great Britain.

0273–1223/92 $15.00

NMR IMAGING OF HYDRODYNAMICS NEAR MICROBIALLY COLONIZED SURFACES

Z. Lewandowski*, S. A. Altobelli**, P. D. Majors*** and E. Fukushima**

**Center for Interfacial Microbial Process Engineering, Montana State University, Bozeman, MT 59717, USA*
***Lovelace Medical Foundation, 2425 Ridgecrest Dr. SE, Albuquerque, NM 87108, USA*
****UNM/NSF Center for Micro-Engineered Ceramics, University of New Mexico, Albuquerque, NM 87131, USA*

ABSTRACT

Nuclear magnetic resonance imaging (NMRI) was used to study fluid flow in a model flow bioreactor as a function of biofilm formation. NMRI in which the phase of the nuclear spins depends on the spin velocity was used to obtain fluid velocity distribution, whereas images predominately of the biofilm density were obtained by spin-lattice relaxation time weighted data. Velocity images showed the manner in which the fluid velocity changed around a biomass growth. We conclude that NMRI is an excellent tool to study these systems.

KEYWORDS

Biofilm, hydrodynamics, flow, nuclear magnetic resonance, NMR, NMRI, MRI.

INTRODUCTION

There are many cases in natural and man-made flows when the growth of bacteria on the solid-liquid interface critically affects the flow. The spatial distribution of the bacteria film in the reactor as a function of time depends on hydrodynamic parameters such as the spatial distribution of velocities and fluctuations. Non-invasive measurements of such parameters are difficult in the presence of biofilm because of the inability of most methods to see through the solid phase.

Nuclear magnetic resonance imaging (NMRI) is a non-invasive method which uses radiofrequency magnetic fields in the presence of a strong static magnetic field to obtain information from an assembly of some specific atomic nuclei, typically hydrogen nuclei or protons, as to its concentration, physical state including flow, chemical environment, etc. NMRI has now become an accepted modality for clinical diagnosis on the basis only of its ability to make concentration images of hydrogen. In this report, we demonstrate the utility of NMRI in the study of biofilm growth in a flow

reactor. Examples are chosen to show the versatility of the method to yield not only the distribution of water but also the distribution of flow velocities and of the biomass. We will, however, defer the discussion of actual biofilm growth as well as a detailed explanation of NMRI to later papers [and in the case of MRI, to references (Pykett, 1982; Morris, 1986; Caprihan and Fukushima, 1990)] although a qualitative description of the latter will be given.

INTERACTIONS BETWEEN BIOFILM GROWTH AND FLOW

The transport of nutrients in a moving liquid is a sum of convective and diffusional fluxes. In most natural systems, suspended bacteria live on the edge of starvation because the nutrient concentration is low. Therefore, it is in the microorganism's best interest to colonize environments where the flux of nutrients is a maximum. Such environments may correspond to regions of high shear or turbulence because diffusional fluxes are increased in such regions.

As a biofilm grows, surface roughness changes, resulting in alteration of wall shear stresses (Schlichting, 1960; Picologlou, et al., 1980; Cunningham, 1989; Siegriest and Gujer, 1985; Bouwer, 1987; Rittman, 1982; Lewandowski and Walser, 1991). The increase in the biofilm thickness alters the roughness which, in turn, changes the flow pattern and presumably alters the flux of nutrients. We show that NMRI can be used to study this complex interaction.

MATERIALS AND METHODS

The polycarbonate reactor had a thin rectangular chamber with a row of four round posts near the inlet end and three more posts downstream to disturb the flow. The chamber's cross-section was 25 x 2 mm and its length was 250 mm. The incoming fluid first came into a 4-mm deep triangular well before going into the chamber. This was done so that the step at the boundary between the well and the chamber would make the flow velocity more uniform across the chamber. [The reactor outline including the posts and the well are shown by the solid contour lines of Figure 1A as well as in the images of Fig. 4, both in the RESULTS AND DISCUSSION section.]

A constant-head gravitational flow system containing a one-liter tank above the reactor and a peristaltic pump to replenish it was constructed. We added a paramagnetic gadolinium solution (Magnevist, Berlex Laboratories, Inc., Wayne, NJ 07470) to the nutrient solution to reduce the spin-lattice relaxation time. Earlier, we determined that a 1% Magnevist solution did not affect the growth rate of a mixed population of microorganisms so that the 0.1% concentration we used during the experiments was benign. The system was continuously aerated and we assume that no major dissolved oxygen gradient existed along the reactor because the hydraulic residence time in the reactor was in the range of seconds.

To initiate biofilm formation, the reactor was inoculated with activated sludge from a municipal waste water treatment plant. The biofilm was fed with a mixture of 200 mg/l glucose and 2 mg/l yeast extract. The average flow velocity during the inoculation process was maintained at 3 cm/s, corresponding to a typical average flow during the NMRI experiments. The flow volume was measured by timed collection of water passing through the reactor. The flow velocity images in the presence of biofilm were obtained 13 to 24 hours after inoculation whereas the distribution of accumulated biomass was evaluated after 24 and 48 hours.

THE NMRI EXPERIMENTS

NMRI depends on the basic phenomenon that nuclear spins, i.e., atomic nuclei which act in many ways like small bar-magnets, precess in a static magnetic field with a frequency that is exactly proportional to the strength of the magnetic field and that NMRI experiments can measure the distribution of nuclei as a function of the precession frequencies. Thus, in the presence of a known static magnetic field gradient, the distribution of the precession frequencies corresponds to a distribution in space along the direction of the gradient. By repeating the experiment with field gradients in different directions, we can obtain one-, two-, or three-dimensional spatial information.

In this experiment, as is done in the vast majority of NMRI experiments at present, we shall examine only nuclei of mobile protons, i.e., of mobile hydrogen atoms. Therefore, we will directly obtain information only about the liquid and not about the biofilm. We will infer the presence of the biofilm by the fact that a water molecule close to the film will have mobility different from that of bulk water and this will affect an NMRI parameter called the spin-lattice relaxation time T_1. Thus, despite the small mass and absolute volume of the biofilm, it will be possible to image its presence.

We performed several classes of NMR experiments to derive information about the location and state of motion of the water and biomass. The first is simply an image in which the intensity is proportional to the total number of mobile hydrogen, i.e., water, nuclei in a volume element of interest (voxel). Such an image for a flowing system was made with standard flow compensated two-dimensional Fourier imaging methods.

We also used experiments that produce images of water which relaxes faster than bulk water; we believe that the highlighted regions correspond to biofilm locations. These experiments are done with T_1-weighted imaging (Morris, 1986) in which the hydrogen nuclei close to the biofilm can be distinguished from those in the bulk by the shorter relaxation times. Another experiment produces images with regions of high velocity highlighted by the inflow of faster, freshly polarized spins from outside the experimental region (Caprihan and Fukushima, 1990).

NMRI flow velocity measurements are sensitive to non-uniformities of the velocity, both spatially and temporally (Caprihan and Fukushima, 1990). In this study, all flows are steady and laminar, based on the lack of phase encoding artifacts. The velocity measurements were made with two different NMR techniques: a sequence which uses a velocity-sensitive refocussing pulse (Cho, et al.,1986) was used to make cross-sectional velocity images averaged over a 2.5 mm thick slice and a dual-echo imaging sequence (Majors, et al., 1990) was employed to obtain velocities averaged over the 2-mm thickness for the entire bioreactor perpendicular to the thin dimension. Both axial and transverse velocity components can be measured in the dual-echo experiments.

Proton NMRI Measurements were performed at 80.34 MHz on a Nalorac QUEST 4300 spectrometer/imaging system with an Oxford superconducting magnet (1.89T, 31 cm horizontal bore) and a 10 cm diameter rf probe. The imaging region is limited by the magnet to a spherical volume of diameter approximately 8 cm.

For the dual-echo experiments, a three rf pulse imaging sequence (T_r-90-τ-109.5-2τ-109.5-τ-acquire) was used with an interpulse spacing τ of 5.0 ms and a repetition delay T_r of 1.0 s. One hundred and twenty-eight complex data points were acquired in the presence of a 0.4 Gauss/cm gradient with a dwell time of 50 μs. Eight repetitions of 64 phase encoding steps (0.025 Gauss/cm increments) were performed so a complete data set was acquired in approximately 10 minutes. The spin-echo (SE) and stimulated echo (STE) arrays, obtained from the dual echo array, were zero-filled to 256 x 256 points, Gaussian filtered, and Fourier transformed to yield a spin density image (from SE array) and a

velocity image (from STE array). The spatial resolution for the images is dictated by the number of sampled points and was approximately 2 mm in the longitudinal direction, and 1 mm in the transverse direction. The velocity range was set for 40 mm/s in any direction but those nuclei exceeding the phase range can often be "unwrapped" modulo 360 degrees to yield the correct velocity.

In the Cho-type velocity experiment, we selected a 2.5-mm thick slice perpendicular to the incoming flow. The resulting image was a map of only the axial velocity component over the 2 x 25 mm cross-section. We acquired a 256 x 128 point data array, did two or four phase-cycles, and used an echo time T_E of 30 ms. This resulted in approximately 20 x 200 measurements in the cross-section or a spatial resolution of around 0.1 mm. Data acquisition required 8 or 16 minutes per velocity image.

RESULTS AND DISCUSSION

This study illustrates several features of NMRI which rely upon the sensitivity of the NMR signal to its physical, chemical, and motional environment. This includes direct measurement of water distribution and velocities, observation of qualitative flow patterns via partial saturation, and the indirect detection of bacterial colonies by the enhanced T_1 relaxation of the surrounding water.

A set of velocity images which were obtained for the reactor in the absence of biofilm is shown in

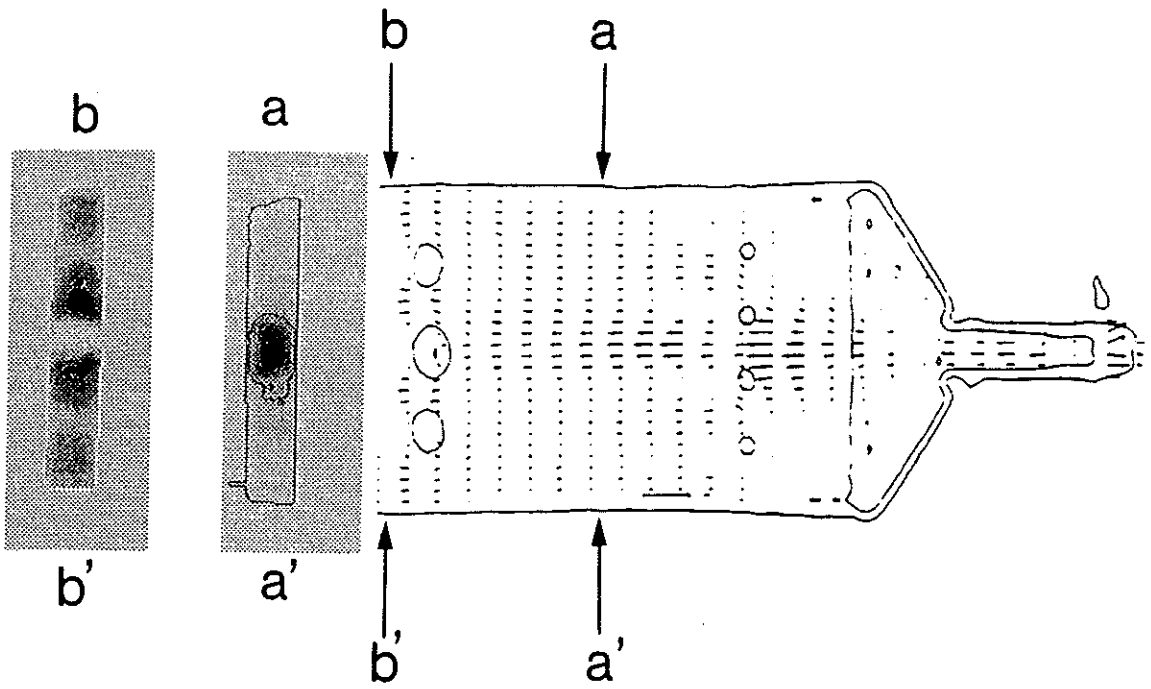

Figure 1 Velocity vectors overlaid with reactor outlines and axial velocity images from two cross-sections.

Fig 1. All of the longitudinal and the transverse images in this report have been rescaled. The right-hand plot is a combination of two dual-echo images (longitudinal and transverse velocity components) in the form of a vector plot. A low resolution, flow-compensated magnitude component is

superimposed on the image to show the geometry (the locations of the posts, walls, and the step) of the reactor. The features that are external to the bioreactor arise from water trapped inside the flow model.

The flow (48 cc/min from right to left) is seen to be symmetric with respect to the bioreactor

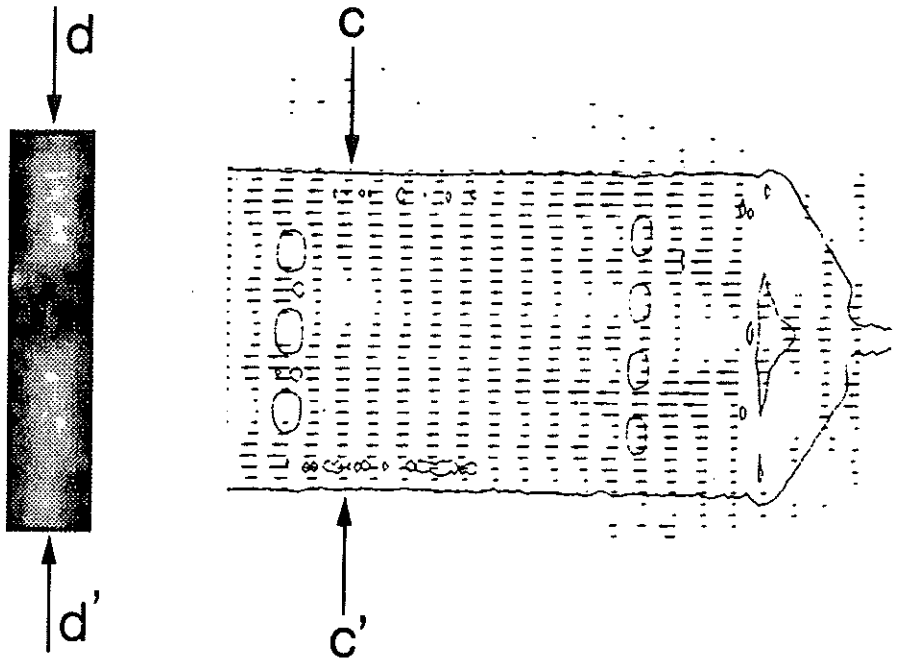

Figure 2 A velocity image of the reactor with biofilm and an axial velocity image through a cross-section through a biomass plug.

symmetry axis. A large jet flows down the center of the bioreactor, with smaller jets passing between the neighboring pairs of posts. A cross-section of the larger jet is clearly seen in the transverse Cho image obtained approximately halfway between the two rows of posts at the arrows marked a-a'. The flow disperses into four jets at the row of three posts, the inner two jets being more intense, immediately downstream of the posts at the arrows b-b'. Although it is difficult to tell from a black and white image, the image also shows reverse, i.e., upstream, velocities near the center post.

A similar series of images which shows the longitudinal velocity for a 30 cc/min flow in the bioreactor obtained ca. 13 hours after inoculation are shown in Fig. 2. The magnitude component is nearly equivalent to that without the biomass but the velocity component is seen to change dramatically, primarily due to large colonies. These colonies, some of which are visible to the eye, are indirectly observable in the images as discrete areas of zero velocity. Several such areas can be seen in the vector plot: one upstream of the row of three posts, one even downstream of the second post from top in the upstream column of posts, and several upstream of the four posts and near the step. Figure 2B is a Cho image taken 12 hours after inoculation approximately 8 mm upstream of the three posts, at the location of a large colony of bacteria at the arrows c-c'. Figure 3 is a velocity profile across the same cut, horizontal through the center of the flow chamber, for 30 and 60 cc/min. The

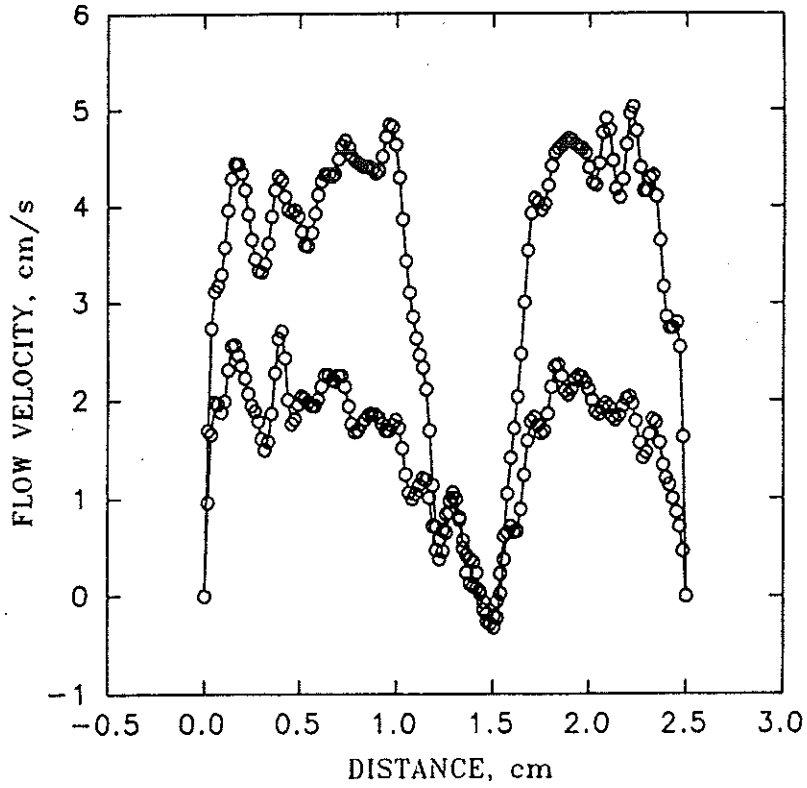

Figure 3 Two velocity profiles through a biomass plug.

fact that the normalized velocity profile at the walls are different from that at the biomass colony (and for that matter, the profiles at the walls with and without the biofilm) might be described in terms of the amount and/or structure of the biomass and will be a subject of a subsequent report.

Figure 4 shows a qualitative way to visualize faster flow pathways. A fast pulse repetition rate causes the faster incoming spins to give a brighter signal than the slower moving spins, whose signal is attenuated (saturated) due to repeated pulsing. Four flow rates (0, 60, 90 and 120 cc/min) are shown in Figs. 4A, 4B, 4C, and 4D, respectively, 18 hours after inoculation. The dark color of the inlet branches for the fastest flow shown (Fig. 4D) is a reflection of nuclear spin dephasing within a voxel probably caused by distribution of velocities. Even though the displays of fast flow are graphic, the dynamic range of this method is limited and, furthermore, the velocity results are not quantitative.

A T_1-weighted image, optimized to cancel the bulk water signal in order to give an image mainly of those nuclei that are close to the bacteria, is shown in Fig. 5. The biofilm, shown in black, has grown predominantly around the well and the upstream side of the posts. Prominent colonies described earlier in connection with Figs. 2 and 4 can be seen near the step, just upstream of the three posts, and downstream of one of the four posts.

Thus, we have seen that NMRI can yield detailed hydrodynamic and density information in a flow system containing biofilm growth. We emphasize that data such as those contained in the velocity

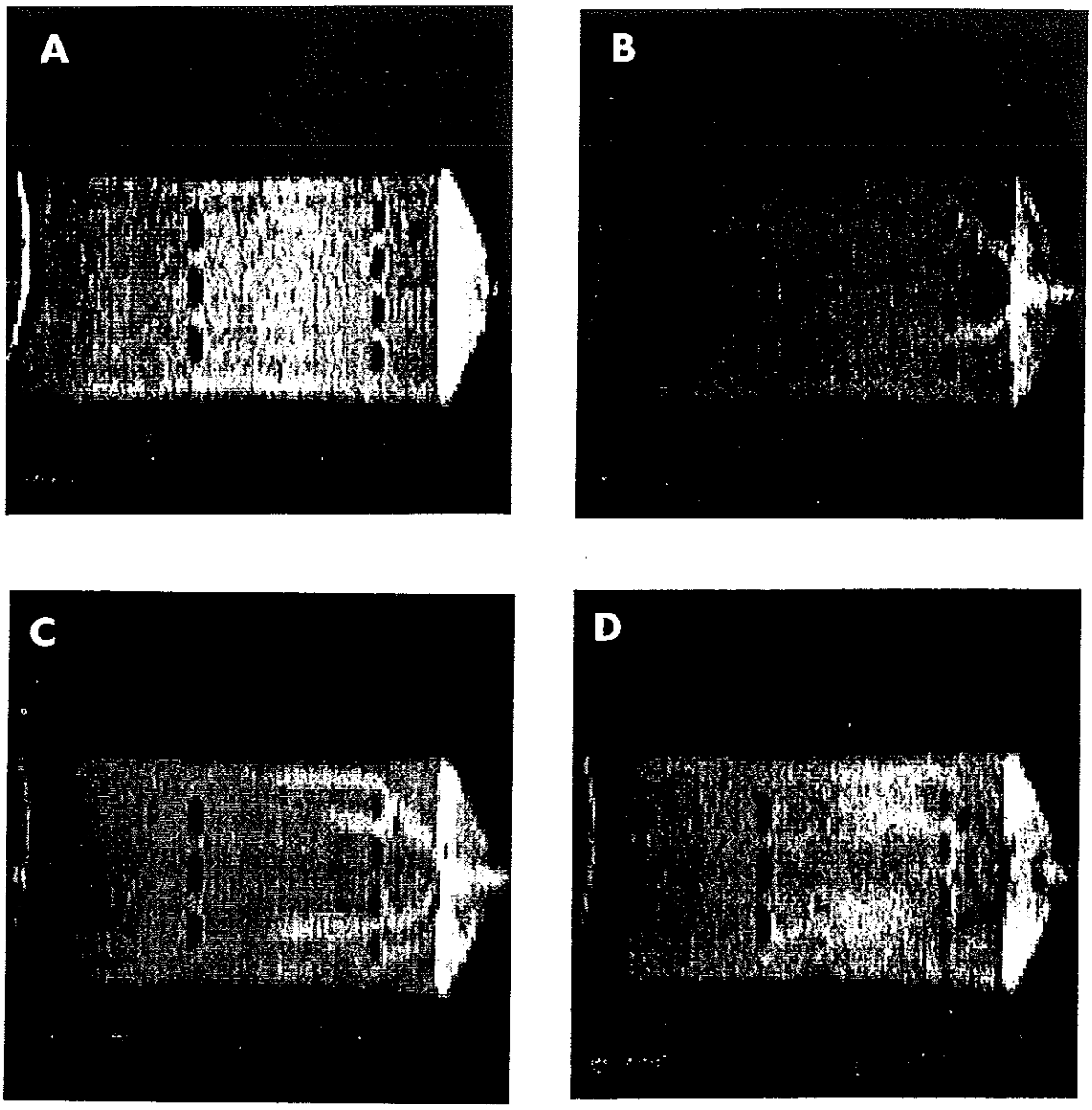

Figure 4 Images showing high velocity regions after 18 hours of biofilm growth. Flow rates are a) 0, b) 30, c) 60, and d) 90 ml/min

images of Figs. 1-3 are quantitative. The fact that the biomass distribution and the flow velocity information can be gathered non-invasively in the same experiment makes NMRI a useful tool for the study of these systems.

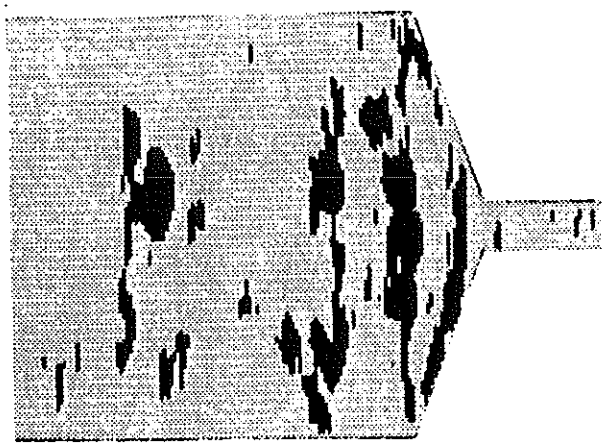

Figure 5 T_1-weighted image showing biofilm accumulation at the step, upstream of both rows of obstacles, and at the location of the "plug".

ACKNOWLEDGEMENT

The authors acknowledge their support from the Center for Interfacial Microbial Process Engineering at Montana State University, a National Science Foundation-sponsored Engineering Research Center, and the Center's Industrial Associates.

REFERENCES

Bouwer E. J. (1987). Theoretical Investigation of Particle Deposition in Biofilm Systems. Water Research 21, 1489-1498.

Caprihan A. and Fukushima E. (1990). Physics Reports 198, 195-235 .

Cho, Z. H., Oh, C. H., Mun, C. W., and Kim, Y. S. (1986). Some results of high flow-velocity NMR imaging using selection gradient. Magnetic Resonance in Medicine 3, 857-862.

Cunningham A. B. (1989). Hydrodynamics and Solute Transport at the Fluid-Biofilm Interface. In: Structure and Function of Biofilms. W. G. Characklis, P. A. Wilderer (Eds). John Wiley, pp. 19-31.

Lewandowski Z. and Walser G. (1991). Influence of shear stress on biofilm thickness. Presented at National Converence on Environmental Engineering. Reno, Nevada, July 8-10.

Majors P. D., Caprihan A, and Fukushima E. (1990). Dual echo flow NMR imaging. 31th Experimental NMR Conference. Asilomar, CA, April.

Morris P. G. (1986). Nuclear Magnetic Resonance Imaging in Medicine and Biology. Clarendon Press, Oxford.

Picologlou B. F., Zelver N. and Characklis W. G. (1980). Biofilm Growth and Hydraulic Performance. Journal of the Hydraulic Division, ASCE 106, No. HY5, 733-746.

Pykett I. L. (1982). NMR Imaging in Medicine. Scientific American 246, 78-88.

Rittman B. E. (1982). The Effect of Shear Stress on Biofilm Loss Rate. Biotechnology and Bioengineering 24, 501-506.

Siegrist H. and Gujer W. (1985). Mass Transfer Mechanism in a Heterotrophic Biofilm. Water Research 19, 1369-1378.